A three-dimensional insight into correlation between carrier lifetime and surface recombination velocity for nanowires

Dingkun Ren[1,*], Zixuan Rong[1], Siddharth Somasundaram[1], Khalifa M. Azizur-Rahman[2], Baolai Liang[1,3] and Diana L. Huffaker[1,2,3]

[1] Department of Electrical and Computer Engineering, University of California, Los Angeles, Los Angeles, California, USA, 90095

[2] School of Physics and Astronomy, Cardiff University, Cardiff, Wales, UK, CF24 3AA

[3] California NanoSystems Institute, University of California, Los Angeles, Los Angeles, California, USA, 90095

[*]Email: dingkun.ren@ucla.edu

Abstract

The performance of nanowire-based devices is predominantly affected by nonradiative recombination on their surfaces, or sidewalls, due to large surface-to-volume ratios. A common approach to quantitatively characterize surface recombination is to implement time-resolved photoluminescence to correlate surface recombination velocity with measured minority carrier lifetime by a conventional analytical equation. However, after using numerical simulations based on a three-dimensional (3-D) transient model, we assert that the correlation between minority carrier lifetime and surface recombination velocity is dependent on a more complex combination of factors, including nanowire geometry, energy-band alignment, and spatial carrier diffusion in 3-D. To demonstrate this assertion, we use three cases—GaAs nanowires, InGaAs nanowires, and InGaAs inserts embedded in GaAs nanowires—and numerically calculate the carrier lifetimes by varying the surface recombination velocities. Using this information, we then investigate the intrinsic carrier dynamics within those 3-D structures. We argue that the conventional analytical approach to determining surface recombination in nanowires is of limited applicability, and that a comprehensive computation in 3-D can provide more accurate analysis. Our study provides a solid theoretical foundation to further understand surface characteristics and carrier dynamics for 3-D nanostructured materials.

Keywords

Nanowire, carrier lifetime, carrier dynamics, surface recombination velocity, TRPL

1. Introduction

The performance of nanowire-based devices is predominantly affected by nonradiative recombination on their surfaces, or sidewalls, due to large surface-to-volume ratios. Nonradiative recombination centers on surfaces, i.e., surface states (or dangling bonds), which are caused by interruptions to the crystal periodicity, leading to higher levels of threshold current and dark current for emitters and detectors, respectively. Such dark current is disadvantageous for energy-efficient and high-temperature operation of emitters and detectors. Thus, it is crucial to quantify the surface property of nanowires in order to explore the impact of surface states on carrier dynamics, allowing for guidance on the design of better nanoscale devices. Typically, the property of surface recombination is interpreted as surface recombination velocity (in units of cm/s). Unfortunately, the characterization of surface recombination velocity for nanowires is far more complicated than for thin films. This is because the three-dimensional (3-D) geometries of nanowires have a larger area of exposed surfaces on different crystal orientations, and therefore analytical solutions cannot be easily found for such nanostructures [1].

One technique commonly used to extract the surface recombination velocity of nanowires is to correlate its value with minority carrier lifetime measured by time-resolved photoluminescence (TRPL). This relation is given by a conventional analytical equation expressed as [2]:

$$\frac{1}{\tau_{TRPL}} = \frac{1}{\tau_{Bulk}} + \frac{4v_S}{d} \tag{1}$$

where τ_{TRPL} is the carrier lifetime measured by TRPL, τ_{Bulk} is the carrier lifetime of the bulk nanowire, v_S is the surface recombination velocity at nanowire-air (or nanowire-passivation interfaces), and d is the nanowire diameter. This analytical approach has been reported in a broad range of studies on nanowire surface properties, including relaxed and strained GaN nanowires without passivation [3], Si nanowires coated by amorphous silicon (a-Si) [4], GaAs nanowires covered by *in-situ* AlGaAs layers [5,6], InGaAs nanopillars passivated by $(NH_4)_2S/SiO_2$ films [7], and InP nanowires passivated by Al_2O_3/PO_x [8]. However, looking back at the original publication that shows the derivation of eq. 1, we note that it is derived based on the assumption that the nanowire is an infinitely long cylinder [2,9]. Naturally, this is not

the case for an actual nanowire, which has hexagonal cross-section (terminated by six (0-11) facets) with a finite height (or length). Therefore, we surmise that eq. 1 might not accurately solve for nanowire v_S and that a comprehensive 3-D computation is required to provide a more accurate analysis.

Here, we have revisited the correlation between carrier lifetime (τ_{TRPL}) and surface recombination velocity (v_S) by reproducing TRPL measurements and numerically solving carrier drift-diffusion with our 3-D transient model. We simulate and analyze three cases using (1) GaAs nanowires, (2) InGaAs nanowires, and (3) InGaAs layer inserts embedded in GaAs nanowires, all of which are on a GaAs substrate to maintain similarity with common nanowire structures [10-13]. The first case considers nanowire structures with no potential barriers between any junctions that would confine minority carriers within the nanowire. The latter two cases are general situations where minority carriers are confined within nanowires because of certain energy-band alignments. Our resultant simulations show that the correlation is convoluted, and is determined not only by recombination on the surface, but also by nanowire geometry, energy-band alignment, and spatial carrier diffusion in 3-D.

The first part of this work involved the validation of our 3-D transient model for nanowire surface recombination by replicating experimental TRPL characterizations of $(NH_4)_2S/SiO_2$ passivated InGaAs/InP nanopillars reported in a previous study [7]. Next, equipped with the modeling capability and the fundamental insight we gained from the first step, we analyze the impact of v_S on τ_{TRPL} for each of the three aforementioned cases. If the conventional analytical correlation stands, the extracted surface recombination velocity (v_S') from the simulated (or measured) τ_{TRPL} based on the relation in eq. 1 should be equal to v_S set in the transient model. However, we observe that v_S' is larger than v_S in most situations with decreasing v_S or increasing d, which indicates that surface recombination velocities derived by eq. 1 are overestimated for the cases investigated in this study. We believe that the complex carrier dynamics in 3-D geometries are responsible for such overestimation. With such structures, the conventional analytical approach is of limited use, and a more comprehensive computation in 3-D can provide more accurate analysis.

2. Modeling and simulation section

2.1. Simulation process

The 3-D computational transient model of the nanowire structure was set up in Synopsys Sentaurus TCAD based on the finite-element method (FEM) to mimic a TRPL measurement process [14]. The output of the simulation was the nanowire's temporal optical emission in response to a laser pulse, caused by band-to-band radiative recombination. A similar model setup was discussed elsewhere [1]. A unit cell of nanowire arrays was first built to include a single nanowire, a dielectric growth mask (SiO_2), a growth substrate (GaAs), and ambient air. However, a growth mask may not be necessary in the model if the nanowire growth is self-assembled instead of selective-area. Figure 1 shows the schematics of the three abovementioned nanowire structures – GaAs nanowire, InGaAs nanowire, and InGaAs insert embedded in GaAs nanowire. Then, the optical generation (in units of cm^{-3} s^{-1}) was computed using finite-difference time-domain (FDTD) method with periodic boundaries specified along the X and Y directions and perfectly matched layer absorbing boundaries specified above and below the nanowire unit cell in the Z direction. Next, the drift-diffusion and continuity equations were solved, and band-to-band radiative recombination of (In)GaAs segments was computed as a function of time to obtain temporal TRPL curves. For a 3-D geometry, the radiative recombination rate (in units of cm^{-3} s^{-1}) has a high dependence on position due to a nonuniform distribution of carriers and can be expressed as:

$$R(x,y,z,t) = B[n(x,y,z,t)p(x,y,z,t) - n_0(x,y,z,t)p_0(x,y,z,t)] \quad (2)$$

where n and p are local carrier densities of electrons and holes, respectively, B is the radiative recombination coefficient, and t is time. Then, the actual time-dependent radiative recombination, i.e., the intensity of photoluminescence emission, from (In)GaAs nanowire segments can be calculated as:

$$I(t) = \int R(x,y,z,t)dV \quad (3)$$

where $I(t)$ is the intensity of optical emission at t and V is the overall volume of the (In)GaAs segments. The Sentaurus TCAD simulator offers the critical benefit of being able to compute Poisson equations in 3-

D structures and solve carrier concentrations in steady states at different points in time. This allows us to directly probe temporal and spatial carrier motion. Finally, τ_{TRPL} was extracted from the simulated TRPL curve that fitted a single decay exponential equation of $\exp(-t/\tau_{TRPL})$. Indeed, we also observed TRPL curves, at high surface recombination velocities ($\geq 10^5$ cm/s), that would require fitting with biexponential decay equation. However, such an analysis was beyond the scope of our current work. Note that we used a low excitation condition in simulations and thus the lifetime τ represented the minority carrier lifetime. We also computationally mapped the spatial and temporal carrier distributions in nanowire segments to reveal the underlying carrier dynamics. To represent an optical excitation from a pulsed laser source, the incident light was set as a Gaussian function with full width at half maximum (FWHM) in the picosecond level. This was based on the calibrated specifications of our TRPL characterization setup using an NKT SuperK EXTREME continuum laser. In a previous study, a similar transient model was applied to exploit multiple material properties, such as carrier mobility, nonradiative recombination lifetime, and surface recombination velocity at the heterointerfaces, for GaAs nanowires grown on Si substrates [1].

2.2. Parameter settings and electrical boundary conditions

The temperature was set at 300 K. When reconstructing unit cells of nanowires in the electrical simulation, we fixed the pitch and height at 600 nm and 1 μm, respectively, and varied the nanowire diameter (d) at 80 nm, 100 nm, 120 nm, 140 nm, and 180 nm. The thickness of the SiO_2 mask was set to 20 nm (this thickness value may vary depending on the growth structure or material). The indium composition of the InGaAs bulk nanowire and insert was set to 0.13, causing an optical emission peak at 1 μm, which was below the cutoff wavelength of the silicon single-photon avalanche diodes. In addition, the lattice mismatch between $In_{0.13}Ga_{0.87}As$ and GaAs was small enough as to not cause any local defects in the nanowires [15]. To simplify the structure, we assumed that the diameter of a nanohole was the same as d, and we excluded from the model the passivation layer that covered the nanowire surfaces. Instead, v_S was introduced at the nanowire-air or nanowire-passivation interfaces on the sidewalls. More details about nanowire dimensions are presented in the Supplementary Information (SI.1).

In the optical simulation, the power intensity of normal incidence was kept fixed at a low level of 10 W/cm^2, which gave a low injection condition. We used a 635 nm wavelength to excite GaAs nanowires and a 965 nm wavelength to excite InGaAs nanowires or inserts. The laser source at 965 nm, which is beyond the cutoff of GaAs, allowed optical generation to occur only in InGaAs segments. Additionally, the refractive index (n) and the extinction coefficient (k) were obtained from previous study [16]. Then, the 3-D optical generation profiles were coupled into the electrical transient simulations. A FWHM of 30 ps was set to time-dependent optical generation, and the entire simulation period is set to 10.0 ns, which provided a fair amount of time to observe TRPL decays (or carrier decays) in each case. To investigate the impact of surface recombination on carrier lifetime v_S was the only material property that was treated as a variable, ranging from 1.0×10^1 cm/s to 1.0×10^4 cm/s (i.e., 1.0×10^1 cm/s, 3.0×10^1 cm/s, 1.0×10^2 cm/s, 3.0×10^2 cm/s, 1.0×10^3 cm/s, 3.0×10^3 cm/s, and 1.0×10^4 cm/s respectively), while all other properties were held constant. Some of the material properties of (In)GaAs segments kept under consideration were (1) electron mobility at 1000 cm^2/(V·s) [17-20], (2) hole mobility at 100 cm^2/(V·s) [17-20], (3) Shockley-Read-Hall (SRH) nonradiative recombination lifetime (for bulk nanowires) at 100 ns [21], and (4) radiative recombination coefficient at 2.0×10^{-10} cm^3/s [14,21]. Note that at the level of mobility given above, the diffusion length of either electron or hole was much longer than the nanowire diameter. All other properties used in the simulations were taken from the material database of the numerical simulator. A summary of all material parameters, including carrier mobilities, doping levels, and radiative recombination coefficients, can be found in the SI. 2.

Another critical aspect of the electrical simulations was to correctly set the boundary conditions. The electrical simulation requires a contact surface with a specified applied voltage; however, the steady states had to be numerically solved at zero bias. Therefore, if the contact was set incorrectly, the carriers may have found the contact and contributed to a photocurrent, rather than recombine at the sidewalls or scatter back into the bulk of the nanowires. As a result, to both appease the simulator and prevent an incorrect simulation, we set both contacts (i.e., the anode and cathode) at the bottom of the substrate with

zero applied voltage. The idea behind this was to ensure that the contact was far away from the nanowire (and the photogenerated carriers), ensuring that the carriers were unlikely to find the contact. Furthermore, the zero applied voltage ensured that no electric field would affect the motion of the carriers.

2.3. Extraction of surface recombination velocity

For each case, there were in total 35 computed TRPL curves with their corresponding carrier lifetimes from resultant transient simulations (five values of d and seven values of v_S). At that moment, we treated v_S as the actual surface recombination velocity at nanowire-air or nanowire-passivation interfaces for an as-grown nanowire sample. To analytically obtain the surface recombination velocity, we fitted v_S by using eq. 1 to estimate its value based on the relation shown below:

$$\tau_{TRPL}{}^{-1} = \left(\frac{4}{d_{eff}}\right) v_S{}' + \tau_{Bulk}{}^{-1} \tag{4}$$

Note that we used v_S' to indicate that the value was an experimentally fitted number based on the conventional analytical model. It should be noted that d_{eff} represents the effective circular cross-section diameter (d_{eff}) by equating its area to that of the actual nanowire hexagonal cross-section area, hence:

$$d_{eff} = \sqrt{\frac{2\sqrt{3}}{\pi}} \cdot d_{EE} = \sqrt{\frac{3\sqrt{3}}{2\pi}} \cdot d_{VV} \tag{5}$$

where d_{EE} and d_{VV} are hexagonal nanowire cross-section edge-to-edge and vertex-to-vertex diameter respectively. All diameters used for calculation in this paper are d_{eff}. This, then, is the entire process of transient simulation for TRPL measurements, and the model can be easily adjusted and modified for any nanowire structure. One assumption we made in the simulation is that all nanowire unit cells are identical. This is reasonable if the nanowire growth is uniform, but the assumption may not hold for non-uniform self-assembled growths with or without catalysts. In such cases, some corrections would be required to modify the model. For instance, a larger unit cell can be used to include multiple nanowires of varying geometrical parameters to approximate a non-uniform array.

2.4. Model validation

To demonstrate the rationality of our transient model for nanowire surface recombination, we validated it by replicating the TRPL characterizations in a surface passivation study by the Fiore's group [7]. They demonstrated a strong suppression of surface recombination of InGaAs/InP nanopillars by using $(NH_4)_2S/SiO_2$ as passivation for InGaAs layers, where TRPL characterizations were performed on a series of nanopillars with different diameters. The best surface recombination velocity fitted by eq. 4 was reported to be 260 cm/s. We reconstructed the same structures using our transient model and obtained a surface recombination velocity of 215 cm/s, which was very close to the measured value. All simulation details are given in SI.3.

3. Results and discussion

3.1. GaAs Nanowires on GaAs Substrates.

We first investigate the correlation between τ_{TRPL} and v_S for bulk GaAs nanowires on GaAs substrates. Again, this case encompasses nanowire growth structures without potential barriers between any junctions to confine minority carriers. Figure 2(a) provides a 3-D map of the optical generation profile at a wavelength of 635 nm for a periodic GaAs nanowire array, where the nanowire pitch and diameter are 600 nm and 120 nm, respectively. Clearly, a large portion of the incident light is concentrated within the nanowires. This is because of optical resonant-guided modes that couple normally incident light into periodic 3-D structures leading to an enhancement of the local electromagnetic field intensity [1,22-25]. Thus, it is fair to assume that the motion of photogenerated carriers are predominantly affected by the nanowire properties. Figure 2(b) illustrates cross-sectional optical generation profiles of unit cells of GaAs nanowires with different diameters, spanning from 80 nm to 180 nm. Note that the photogenerated carriers are not uniformly distributed—there are several "hot spots" inside the nanowires. The rapid separation of electrons and holes at the beginning, caused by the difference between their carrier mobilities, will result in an abrupt decay of the TRPL curve (an exception is when electron mobility and hole mobility are

reasonably close within one order). A similar mechanism is discussed in a study on thin-film CdTe solar cells, where the first part of decay in a biexponential TRPL curve is attributed to rapid carrier separation [26].

Next, we move on to the analysis of the electrical simulations. Figure 3 displays the simulated carrier lifetimes and TRPL curves for GaAs nanowires. The top-left contour plot shows the correlation between carrier lifetimes and two nanowire properties: v_S and d. The carrier lifetime is also expressed by three contour lines at 0.70 ns, 0.80 ns, and 0.90 ns. Four subplots show simulated TRPL curves by fixing v_S at 1×10^1 cm/s, 1×10^2 cm/s, 1×10^3 cm/s, and 1×10^4 cm/s. Since all TRPL curves behave as single exponential decays, we extract their corresponding τ_{TRPL} by fitting $\exp(-t/\tau_{TRPL})$ from 2 ns to 5 ns (the curves from 5 ns to 10 ns are not shown). We observe that the extracted τ_{TRPL} is less than 1 ns, regardless of the v_S and d combination. We also note that as v_S decreases, d exhibits a more significant impact on τ_{TRPL}, while v_S becomes the dominant factor in the regime where v_S is greater than 1×10^3 cm/s.

To understand the underlying physics of carrier behaviors, it is crucial to first recognize that a large portion of carriers are more likely to gradually diffuse from nanowire segments into substrates when there are no potential barriers at the nanowire-substrate interfaces for minority carriers. In other words, carriers are unlikely to recombine on surfaces while the entire system is "open". This could potentially explain why the experimentally measured τ_{TRPL} for GaAs nanowires grown on GaAs, which has no potential barrier, is within a picosecond or nanosecond regardless of nanowire diameter or surface passivation condition [5,6,27]. However, it is still possible to obtain a longer τ_{TRPL} when (1) the nonradiative SRH recombination lifetime of the bulk GaAs nanowires is long, (2) the carrier mobility is low (or the diffusion length is small), (3) d is large, or (4) the TRPL signals are mixed with optical emission from the substrate. With decreasing d, most of the photogenerated carriers recombine on the nanowire surfaces due to the high surface to volume ratio of the nanowire, and thus the fraction of carriers that diffuse into substrates are much lower.

After obtaining carrier lifetimes, we start to examine the rationality of the conventional analytical model for nanowire surface recombination velocity, or eq. 4. Again, v_S is the surface recombination velocity

we input into the transient simulations, and thus can be considered the "actual" recombination velocity at the nanowire-air or nanowire-passivation interfaces. To analytically extract v_S' using eq. 4, we plot the simulated τ_{TRPL}^{-1} as a function of d^{-1} by fixing v_S at 1×10^1 cm/s, 1×10^2 cm/s, 1×10^3 cm/s, and 1×10^4 cm/s, as shown in subplots a, b, c, and d, respectively, in figure 4. The fitted values of v_S' for those four values of v_S are 3.97×10^2 cm/s, 4.92×10^2 cm/s, 1.45×10^3 cm/s, and 7.23×10^3 cm/s, respectively. We then summarize the values of v_S and v_S', as illustrated in the top-left plot in figure 4, where the dashed grey line is the ideal relation between v_S and v_S' (i.e. $v_S = v_S'$). We notice that v_S' becomes much larger than v_S when v_S is smaller than 1×10^3 cm/s, suggesting that eq. 4 overestimates surface recombination velocities in that regime.

Recall that eq. 1 (or eq. 4) was analytically derived based on the assumption that the nanowire is an infinitely long cylinder. Looking back at the literature, we find that eq. 1 was first derived to calculate the carrier concentration of InGaAs quantum dots by using two-dimensional (2-D) continuity and boundary conditions [2,9]. However, these boundary conditions are not appropriate for the case of nanowires, which are 3-D. More importantly, the traditional analytical argument does not consider carrier diffusion into substrates when there are no potential barriers at nanowire-substrate interfaces. As a result, the entire radiative recombination rate, according to eq. 2, or the intensity of the optical emission, eq. 3, will suffer from an abrupt decay, and the calculated v_S' becomes large. However, the rapid diffusion of the carriers into the substrate will lead to a significant loss of photogenerated carriers within the nanowire segments, meaning that v_S' may not necessarily be large. In other words, the higher actual value of v_S' can be attributed to either carrier diffusion or a poor surface.

To provide further insight into the carrier dynamics and recombination mechanisms, we map the temporal and spatial distribution of the minority carriers, or holes, across an entire GaAs nanowire unit cell. Figure 5 shows the simulated hole distribution for $v_S = 1\times10^2$ cm/s and 1×10^4 cm/s at different times, namely 10 ps, 30 ps, 50 ps, 70 ps, 100 ps, 500 ps, and 1000 ps. Note that the photogenerated carriers are mostly confined within the nanowire segments. At the beginning (from 0 ps to 70 ps), right when the laser pulse (Gaussian profile) arrives, the density of the photogenerated minority carriers increases for both values of

v_S. Meanwhile, the holes in the nanowire segments rapidly diffuse to the sidewalls and substrate. However, after 70 ps, the two cases show significant differences in their carrier distribution profiles. After 1000 ps, the profile with the lower v_S (1×10^2 cm/s) shows significantly more carriers than the one with the higher v_S ($1x10^4$ cm/s). This agrees with our previous observation that the decay of the TRPL intensity becomes more dependent on surface recombination with increasing v_S.

3.2. ***InGaAs nanowires and InGaAs inserts in GaAs nanowires on GaAs substrates***

Turning now to the InGaAs nanowires and InGaAs inserts in GaAs nanowires, we first look at the optical generation in both cases, as shown in figure 6(a). Since the excitation wavelength (965 nm) is beyond the cutoff wavelength of GaAs, all carriers are generated inside InGaAs segments. Note that InGaAs-GaAs forms a type-I heterojunction, as illustrated in figure 6(a), and thus photogenerated carriers are mostly confined in the InGaAs segment without diffusing away to the GaAs segment. More information regarding the optical generation profiles are given in SI.4. Although, carrier diffusion would still occur due to thermionic emission, the fraction of carriers is much lower than that in the GaAs nanowires discussed in the previous case. As done for the previous structure, we analytically extract v_S' using eq. 4 with v_S ranging from 1×10^1 cm/s to 1×10^4 cm/s, as shown in figure 6(b). We note that the discrepancy between v_S and v_S' is much less in this case (more details of analytical fittings are provided in the SI.4). Such a difference is attributable to the recombination at the top and bottom surfaces of the InGaAs segments, i.e., the top InGaAs-air interface and the bottom InGaAs-GaAs (nanowire-substrate) heterointerfaces in the case of the InGaAs bulk nanowires, and both the top and bottom InGaAs-GaAs heterointerfaces in the case of the InGaAs inserts in GaAs nanowires. Since the lattice mismatch between $In_{0.13}Ga_{0.87}As$ and GaAs is small, the surface recombination velocity at the heterointerfaces would be much smaller than at the semiconductor-air interfaces, resulting in a significant fraction of carriers recombining at the nanowire sidewalls (semiconductor-air interface) similar to that of the infinite nanowire, where all the carriers recombine at the nanowire sidewalls. As a result, the conventional analytical model is valid for this case. Regardless, when v_S is smaller than 1×10^2 cm/s, v_S' will still be slightly overestimated. Figure 6(c) shows contour plots of computed τ_{TRPL} for both cases. Compared with the distribution of τ_{TRPL} for GaAs nanowires

shown in figure 4, the ones given in figure 6(c) show less dependence on d, indicating, again, that the carrier diffusion into the substrate and the surface recombination on top or bottom surfaces are less significant than surface recombination at the nanowire side walls.

3.3. Conditions of reasonable applicability of the analytical model

Equipped with a comprehensive understanding of the correlation between τ_{TRPL} and v_S, we can critique the applicability of the conventional analytical model. In most cases, a fair conclusion cannot be made about the quality of nanowire surfaces without a complete analysis of the carrier dynamics in 3-D by considering the actual geometry of the nanowire. It is more reasonable to analytically solve v_S for thin films, since they can be simply considered as 1-D slices by assuming that the in-plane areas are infinite. In other words, setting electrical boundary conditions in 1-D is more straightforward. However, for 3-D nanowire structures we summarize several conditions for the reasonable applicability of the analytical model presented in eq. 1 (or eq. 4): (1) the nanowire aspect ratio (L/D) is extremely high so as to assume it "infinitely" long; (2) the diffusion length of the minority carriers is much longer than the nanowire d, and therefore the carriers can reach surfaces before being recombined by other bulk nonradiative mechanisms. (3) the minority carriers can be mostly confined within the nanowire segment resulting from certain energy-band alignments; (4) the carrier diffusion into substrates is low; (5) the recombination at both the top and bottom interfaces of the nanowire segment is much less significant than the surface recombination on the sidewalls. Thus, it is critical to carefully consider these prerequisites before implementing the analytical model to solve surface recombination velocities for nanowires. Regardless, eq. 1 (or eq. 4) can still obtain an approximate upper limit of the surface recombination velocity, or, in other words, the worst possible surface recombination velocity, for the nanowire cases studied here.

4. Conclusion

We applied a 3-D transient model to carry out a thorough numerical investigation of the correlation between carrier lifetime and surface recombination velocity for nanowire time-resolved photoluminescence characterizations. We questioned the conventional analytical model that is widely implemented to interpret

such correlation. The conclusion is rather straightforward: with the analytical model, the extracted surface recombination velocity is normally overestimated, and this flaw can be corrected by performing complete 3-D transient modeling. To arrive at this insight, we simulated three common nanowire structures—a GaAs nanowire, an InGaAs nanowire, and an InGaAs insert in GaAs nanowire—and then computationally explored the impact of surface recombination velocity on carrier lifetime. We found, based on the resultant simulations, that the actual correlation was convoluted and determined by not only surface recombination but also by nanowire geometry, energy-band alignment at the heterointerface, and spatial carrier diffusion in 3-D nanostructures. We believe the theoretical work will stimulate more validating studies for carrier dynamics in nanostructured materials and guide the design of nanoscale devices.

Acknowledgements

We gratefully acknowledge the support for this research from the National Science Foundation (grant no. ECCS-1509801) and Sêr Cymru National Research Network in Advanced Engineering and Materials.

ORCID iDs

Dingkun Ren https://orcid.org/0000-0001-9470-1956

Baolai Liang https://orcid.org/0000-0002-2192-9340

Supplementary Information

Detailed dimensions of nanowire unit cells, a summary of parameter settings in optical and electrical simulations, validation of the 3-D transient model for nanowire surface recombination by replicating the TRPL characterizations shown in the passivation study by Fiore's group, optical generation profiles for InGaAs nanowires and InGaAs inserts, more details of analytical fittings for the cases of InGaAs nanowires and InGaAs inserts.

Notes

The authors declare no competing financial interest.

References

[1] Ren D, Scofield A C, Farrell A C, Rong Z, Haddad M A, Laghumavarapu R B, Liang, B and Huffaker D L 2018 Exploring time-resolved photoluminescence for nanowires using a three-dimensional computational transient model *Nanoscale* **10** 7792-802

[2] Allen J E, Hemesath E R, Perea D E, Lensch-Falk J L, Li Z Y, Yin F, Gass M H, Wang P, Bleloch, A L, Palmer R E and Lauhon L J 2008 High-resolution detection of Au catalyst atoms in Si nanowires *Nat. Nanotechnol*. **3** 168

[3] Schlager J B, Bertness K A, Blanchard P T, Robins L H, Roshko A and Sanford N A 2008 Steady-state and time-resolved photoluminescence from relaxed and strained GaN nanowires grown by catalyst-free molecular-beam epitaxy *J. Appl. Phys.* **103** 124309

[4] Dan Y, Seo K, Takei K, Meza J H, Javey A and Crozier K B 2011 Dramatic reduction of surface recombination by in Situ surface passivation of silicon nanowires *Nano Lett.* **11** 2527-32

[5] Chang C-C, Chi C-Y, Yao M, Huang N, Chen C-C, Theiss J, Bushmaker A W, LaLumondiere S, Yeh T-W, Povinelli M L, Zhou C, Dapkus P D and Cronin S B 2012 Electrical and optical characterization of surface passivation in GaAs nanowires *Nano Lett.* **12** 4484-9

[6] Jiang N, Gao Q, Parkinson P, Wong-Leung J, Mokkapati S, Breuer S, Tan H H, Zheng C L, Etheridge J and Jagadish C 2013 Enhanced minority carrier lifetimes in GaAs/AlGaAs core–shell nanowires through shell hrowth optimization *Nano Lett.* **13** 5135-40

[7] Higuera-Rodriguez A, Romeira B, Birindelli S, Black LE, Smalbrugge E, van Veldhoven PJ, Kessels W M M, Smit M K and Fiore A 2017 Ultralow surface recombination velocity in passivated InGaAs/InP nanopillars *Nano Lett.* **17** 2627-33

[8] Black L E, Cavalli A, Verheijen M A, Haverkort J E M, Bakkers E P A M and Kessels W M M 2017 Effective surface passivation of InP nanowires by atomic-layer-deposited Al2O3 with POx interlayer *Nano Lett.* **17** 6287-94

[9] Daiminger F X, Schmidt A, Faller F and Forchel A W B 1994 Picosecond time-resolved investigations of carrier lifetime and carrier capture in InGaAs/GaAs quantum dots *Proc. SPIE* **2139** 213-21

[10] Noborasaka J, Motohisa J and Fukui T 2005 Catalyst-free growth of GaAs nanowires by selective-area metalorganic vapor-phase epitaxy *Appl. Phys. Lett.* **86** 213102

[11] Kim H, Ren D, Farrell A C and Huffaker D L 2018 Catalyst-free selective-area epitaxy of GaAs nanowires by metal-organic chemical vapor deposition using triethylgallium *Nanotechnology* **29** 085601

[12] Yoshimura M, Tomioka K, Hiruma K, Hara S, Motohisa J and Fukui T 2010 Growth and characterization of InGaAs nanowires fored on GaAs(111)B by selective-area metal organic vapor phase epitaxy *Jpn. J. Appl. Phys.* **49** 04DH08

[13] Shapiro J N, Lin A, Wong P S, Scofield A C, Tu C, Senanayake P N, Mariani G, Liang B L and Huffaker D L 2010 InGaAs heterostructure formation in catalyst-free GaAs nanopillars by selective-area metal-organic vapor phase epitaxy *Appl. Phys. Lett.* **97** 243102

[14] Synopsys 2013 TCAD Centaurs Suite, version I-2013.12.

[15] Glas F 2006 Critical dimensions for the plastic relaxation of strained axial heterostructures in free-standing nanowires *Phys. Rev. B* **74** 121302

[16] Adachi S 1989 Optical dispersion relations for GaP, GaAs, GaSb, InP, InSb, AlxGa1-xAs, and In1-xGaxAsyP1-y *J. Appl. Phys.* **66** 603040

[17] Parkinson P, Joyce H J, Gao Q, Tan H H, Zhang X, Zou J, Jagadish C, Herz L M and Johnston M B 2009 Carrier lifetime and mobility enhancement in nearly defect-free core−shell nanowires measured using time-resolved terahertz spectroscopy *Nano Lett.* **9** 3349-53

[18] Joyce H J, Parkinson P, Jiang N, Docherty C J, Gao Q, Tan H H, Jagadish C, Herz L M and Johnston M B 2014 Electron mobilities approaching bulk limits in "surface-free" GaAs nanowires *Nano Lett.* **14** 5989-94

[19] Kinzel J B, Schülein F J R, Weiß M, Janker L, Bühler D D, Heigl M, Rudolph D, Morkötter S, Döblinger M, Bichler M, Abstreiter G, Finley J J, Wixforth A, Koblmüller G and Krenner H J 2016 The native material limit of electron and hole mobilities in semiconductor nanowires *ACS Nano* **10** 4942-53

[20] Farrell A C, Senanayake P, Meng X, Hsieh N Y and Huffaker DL 2017 Diode Characteristics Approaching Bulk Limits in GaAs Nanowire Array Photodetectors *Nano Lett.* **17** 2420-5

[21] GaAs electrical properties
Available from: http://www.ioffe.ru/SVA/NSM/Semicond/GaAs/electric.html.

[22] Mariani G, Scofield A C, Hung C-H and Huffaker D L 2013 GaAs nanopillar-array solar cells employing in situ surface passivation *Nat. Commun.* **4** 1497

[23] Azizur-Rahman K M and LaPierre R R 2015 Wavelength-selective absorptance in GaAs, InP and InAs nanowire arrays *Nanotechnology* **26** 295202

[24] Azizur-Rahman K M and LaPierre R R 2016 Optical design of a mid-wavelength infrared InSb nanowire photodetector *Nanotechnology* **27** 315202

[25] LaPierre R R, Robson M, Azizur-Rahman K M and Kuyanov P 2017 A review of III–V nanowire infrared photodetectors and sensors *J. Phys. D*: *Appl. Phys.* **50** 123001

[26] Kanevce A, Levi D H and Kuciauskas D 2014 The role of drift, diffusion, and recombination in time-resolved photoluminescence of CdTe solar cells determined through numerical simulation. *Prog. Photovolt.*: *Res. Appl.* **22** 1138-46

[27] Burgess T, Saxena D, Mokkapati S, Li Z, Hall C R, Davis J A, WangY, Smith L M, Fu L, Caroff P, Tan, H H and Jagadish C 2016 Doping-enhanced radiative efficiency enables lasing in unpassivated GaAs nanowires *Nat. Commun.* **7** 11927

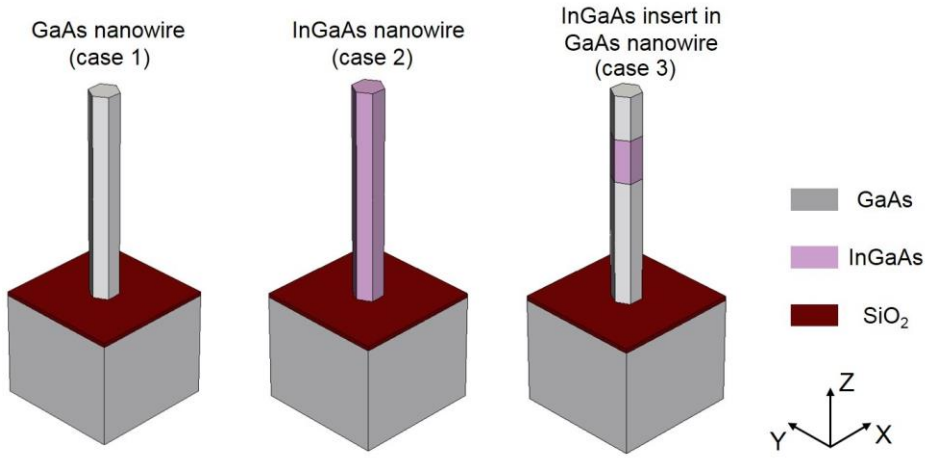

Figure 1. Schematic diagrams of three nanowire structures used in the simulations: GaAs nanowire, InGaAs nanowire, and InGaAs insert embedded in GaAs nanowire. All nanowires are on GaAs substrates. For each structure, only a unit cell is shown.

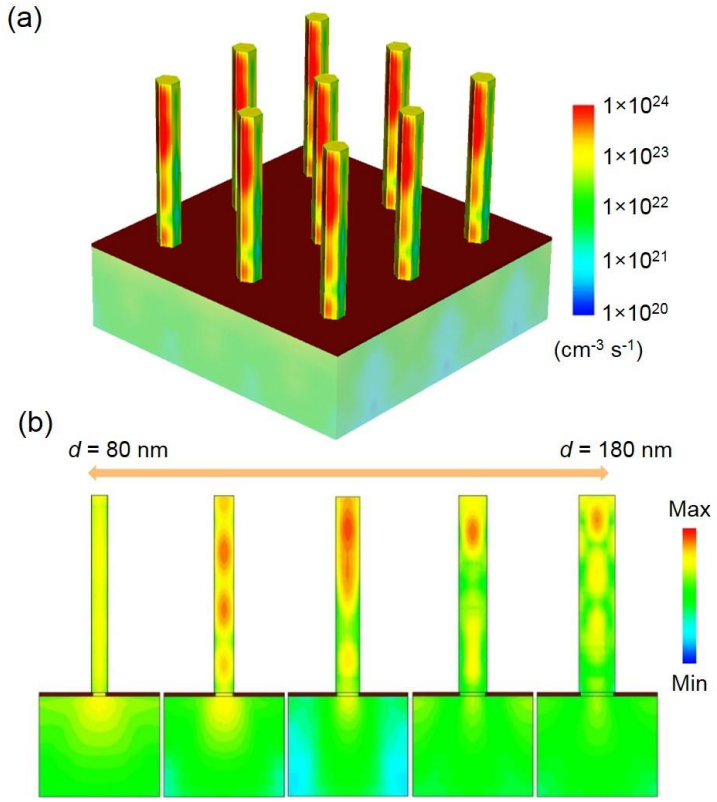

Figure 2. (a) 3-D optical generation profile of a periodic GaAs nanowire array under the incident light (a plane wave) at 635 nm. The nanowire diameter is 120 nm. (b) Cross-sectional optical generation profiles of GaAs nanowires with diameters (each 20 nm larger than the previous) spanning from 80 nm to 180 nm.

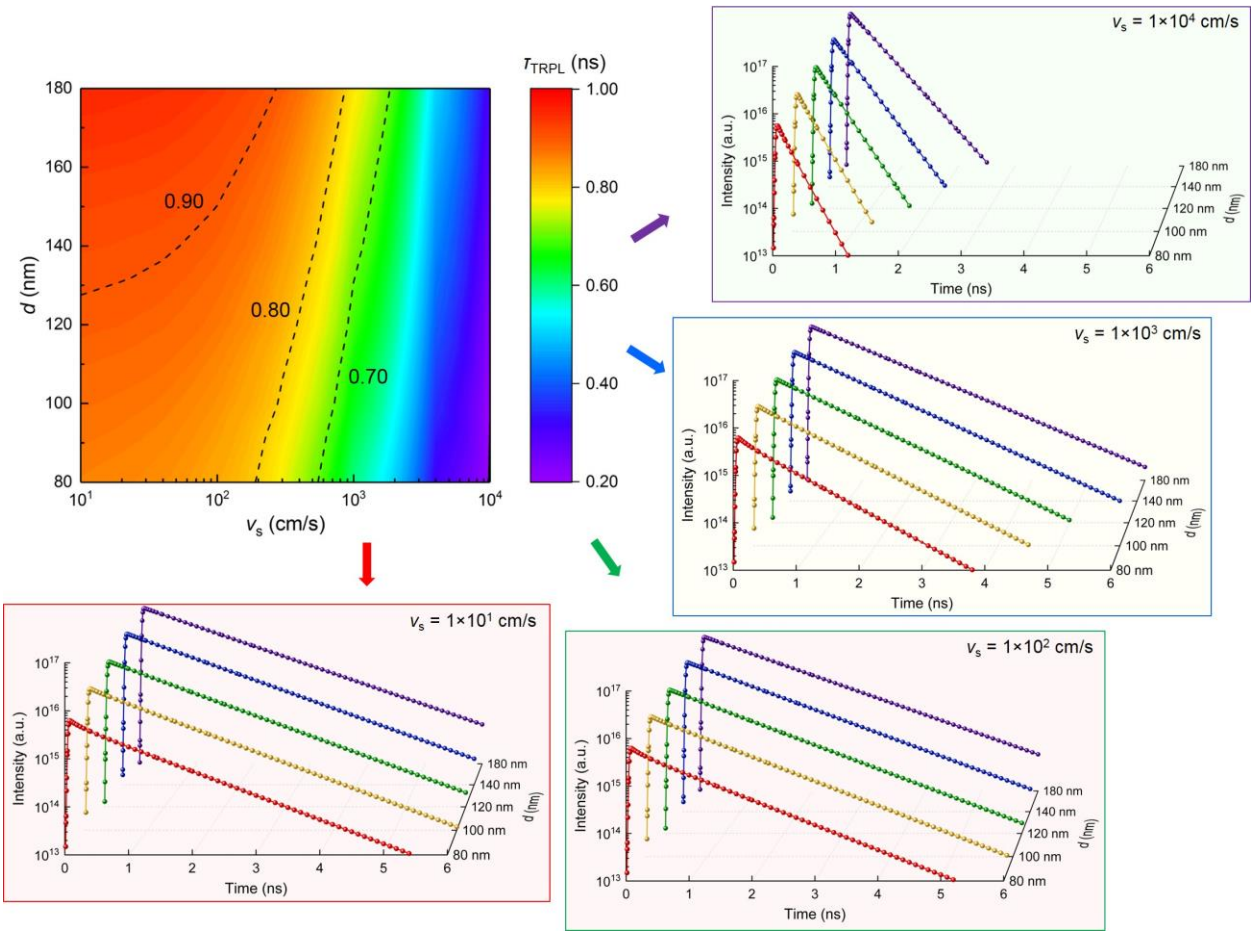

Figure 3. Simulated carrier lifetime and TRPL curves for GaAs nanowires on GaAs substrates as a function of surface recombination velocity and nanowire diameter. The contour plot displays a summary of the distribution of τ_{TRPL}, where the three contour lines correspond to the lifetimes of 0.70 ns, 0.80 ns, and 0.90 ns. Four subplots show simulated TRPL curves for fixed v_S of 1×10^1 cm/s, 1×10^2 cm/s, 1×10^3 cm/s, and 1×10^4 cm/s.

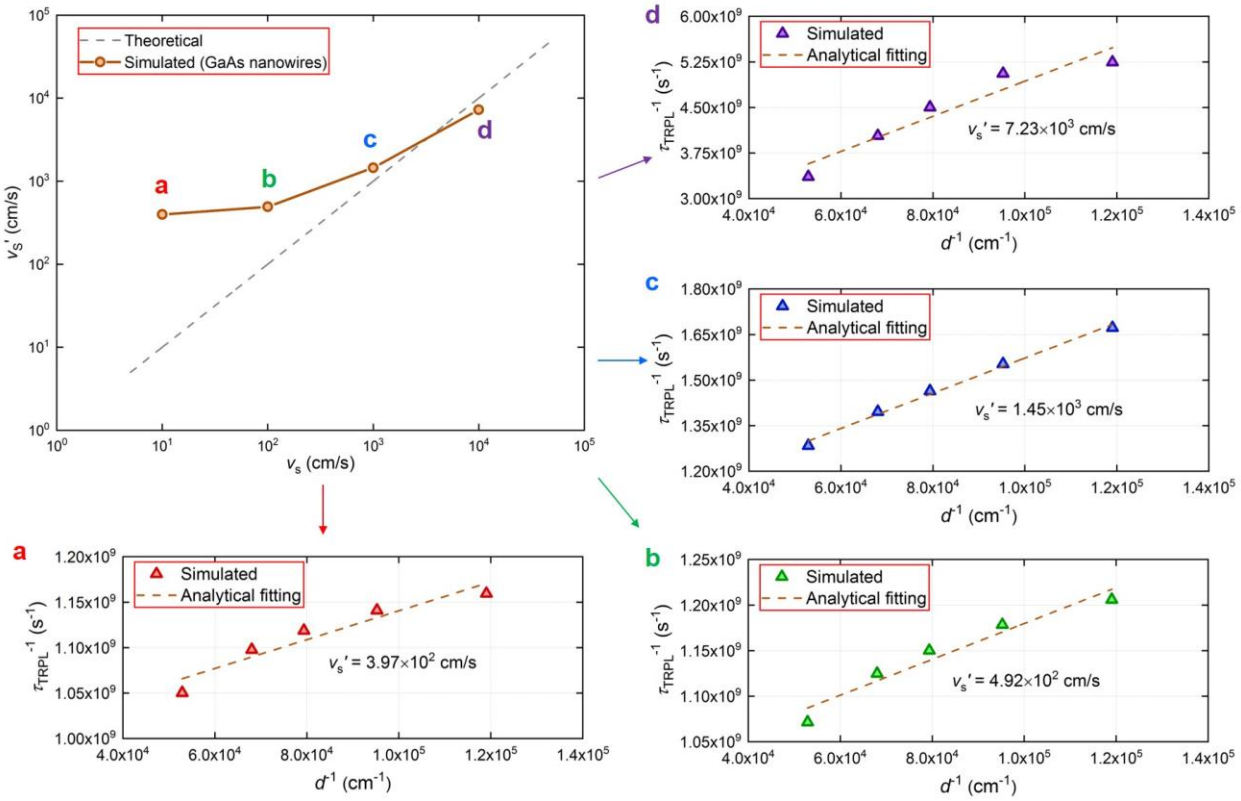

Figure 4. Extracted surface recombination velocity (v_S') versus actual surface recombination velocity (v_S), where v_S represents the value used in the simulations (or the actual surface property) and v_S' is the fitted value using the analytical argument given in eq. 4. The dashed line in the top-left plot shows an ideal relation between v_S' and v_S. The fitted surface recombination velocities v_S' for $v_S = 1\times10^1$ cm/s to 1×10^4 cm/s are depicted in subplots a – d: where $v_S' = 3.97\times10^2$ cm/s, 4.92×10^2 cm/s, 1.45×10^3 cm/s, and 7.23×10^3 cm/s, respectively.

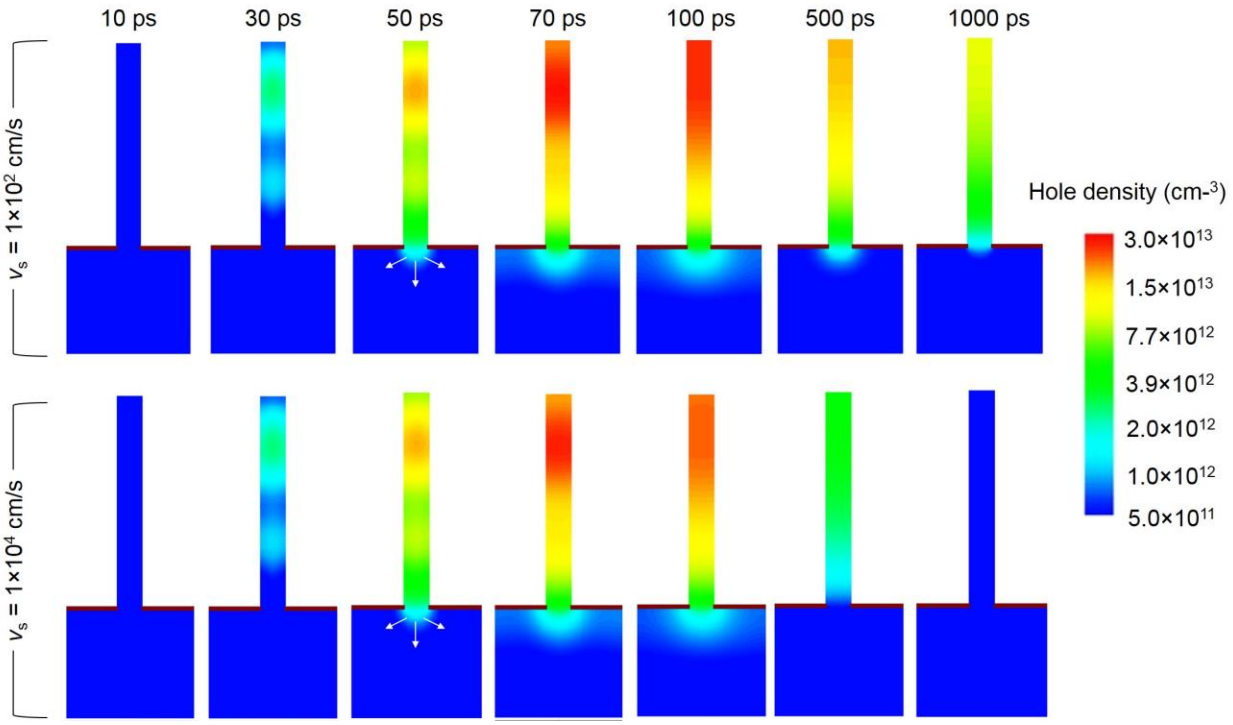

Figure 5. Simulated spatial distributions of minority carriers, or holes, in GaAs nanowires for v_S = 1×10^2 cm/s and 1×10^4 cm/s at different points in time: 10 ps, 30 ps, 50 ps, 70 ps, 100 ps, 500 ps, and 1000 ps. The nanowire diameter is 120 nm. The white arrows indicate the direction of carrier diffusion.

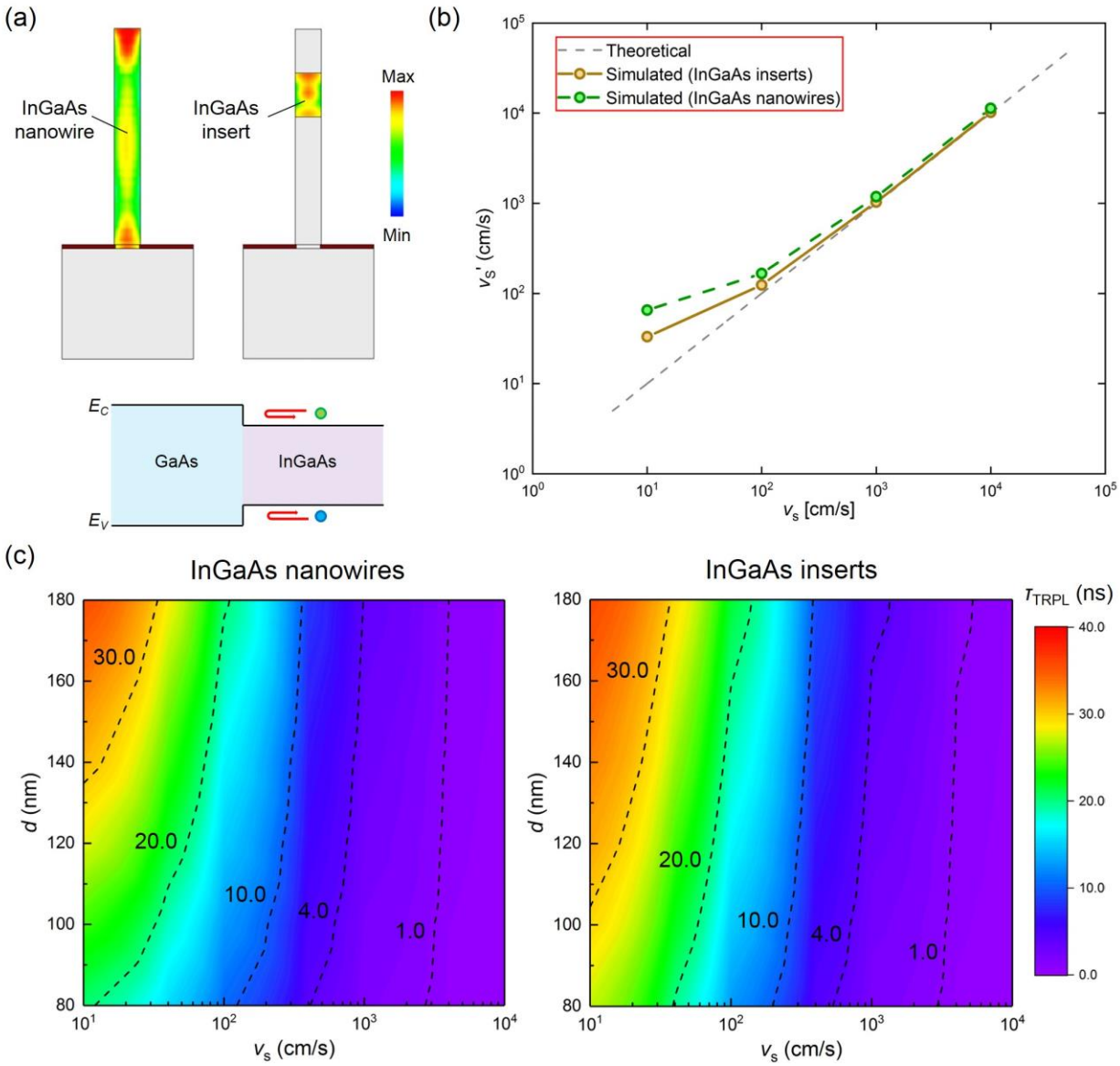

Figure 6. The resultant simulations for the case of InGaAs nanowires and of InGaAs inserts in GaAs nanowires. (a) Cross-sectional optical generation profiles of unit cells for both cases with a nanowire *d* of 120 nm. The schematics on the bottom show the energy-band alignment (type-I) of an InGaAs-GaAs heterojunction, where carriers are confined in the InGaAs segment. (b) Extracted surface recombination velocity (v_S') versus actual surface recombination velocity (v_S). (c) Contour plots of simulated carrier lifetimes for InGaAs nanowires and InGaAs inserts in GaAs nanowires, respectively, as a function of v_S and *d*, where the five contour lines correspond to lifetimes of 1.0 ns, 4.0 ns, 10.0 ns, 20.0 ns, and 30.0 ns.